ACS central science

http://pubs.acs.org/journal/acscii

Research Article

Sustainable Coproduction of Two Disinfectants via Hydroxide-Balanced Modular Electrochemical Synthesis Using a Redox Reservoir

Rui Wang, Hongyuan Sheng, Fengmei Wang, Wenjie Li, David S. Roberts, and Song Jin*

Cite This: *ACS Cent. Sci.* 2021, 7, 2083–2091

Read Online

ACCESS | Metrics & More | Article Recommendations | Supporting Information

ABSTRACT: Challenges posed by the sacrificial auxiliary reactions and expensive ion-exchange membranes in conventional electrosynthesis necessitate developing new electrochemical processes to enable efficient and sustainable distributed electrochemical manufacturing. Modular electrochemical synthesis (ModES) using a redox reservoir (RR) offers a promising membrane-free approach to improve energy efficiency and reduce waste through the pairing of multiple independent oxidative and reductive half-reactions; however, undesired ion-imbalance and induced pH changes in the existing ModES process limit sustained production. Here we present $Ni(OH)_2$ as a heterogeneous RR that can selectively store and transport the hydroxide ions involved in the target half-reactions by reversible conversion with NiOOH to enable an ion-balanced ModES of two common disinfectants, hydrogen peroxide (H_2O_2) and sodium hypochlorite (NaClO). This hydroxide-balanced ModES realizes stable operation without appreciable pH swing to accumulate practically useful concentrations of H_2O_2 and NaClO up to 251 and 481 ppm, respectively. These results illustrate additional design principles for electrosynthesis without sacrificial auxiliary reactions and the need for ion-selective RRs for modular electrochemical manufacturing.

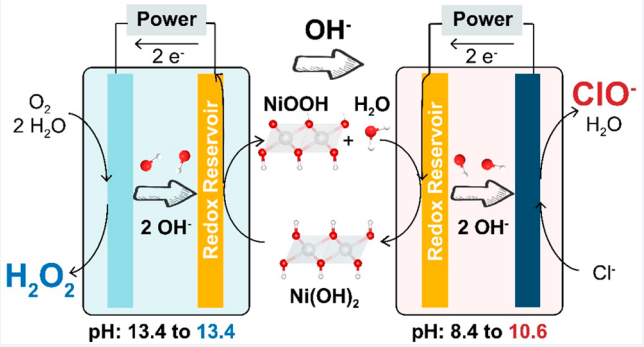

INTRODUCTION

Chemical disinfectants, such as sodium hypochlorite (NaClO, bleach) and hydrogen peroxide (H_2O_2), are routinely used for cleaning and disinfection in many public spaces, such as hospitals and schools, and households.[1,2] Conventional disinfectant production via centralized chemical manufacturing produces highly concentrated chemicals at central plants, which are then distributed to multiple points-of-use by external supply chains and diluted to relatively low concentrations for disinfection applications.[3−6] However, fragile supply chains that arise from relatively high transportation costs and inflexible manufacturing conditions of these disinfectants struggle to cater to their fluctuating demand, and thus have motivated distributed chemical manufacturing with dispersed facilities close to their end-use destinations.[7−11] Distributed on-site production could also provide opportunities to meet the increased local demand for disinfectants during the coronavirus disease (COVID-19) pandemic. In fact, electrochemical devices for producing bleach are commercially available, such as the on-site electrochemical NaClO generators (SANILEC) by De Nora for offshore oil extraction facilities.[12,13] In such a conventional device, hydrogen evolution reaction (HER, $2H_2O + 2e^- \rightarrow H_2 + 2OH^-$) works as the sacrificial half-reaction to supply OH^- for the NaClO generation ($Cl^- + 2OH^- \rightarrow H_2O + ClO^- + 2e^-$). Even though hydrogen gas could be industrially useful, it is comparatively less valuable and undesired as a byproduct during disinfectant production and may cause explosion hazards in point-of-use settings. Therefore, a new electrochemical strategy to pair the useful electrochemical half-reactions for disinfectant production without wasted by-products is desirable.

Modular electrochemical synthesis (ModES) using a redox reservoir (RR)[14] is promising for next-generation distributed electrochemical manufacturing by pairing two half-reactions with the RR reduction or oxidation to decouple the simultaneous electrolysis and avoid the product crossover without the use of a membrane. RRs allow temporary storage of the electrons and ions to redirect them for carrying out different electrochemical half-reactions, possibly at different times, locations, rates, and scales of the reactions. Solid-state RRs are energy storage materials that could serve as interchangeable counter electrodes for either anodic or

Received: September 22, 2021
Published: December 4, 2021

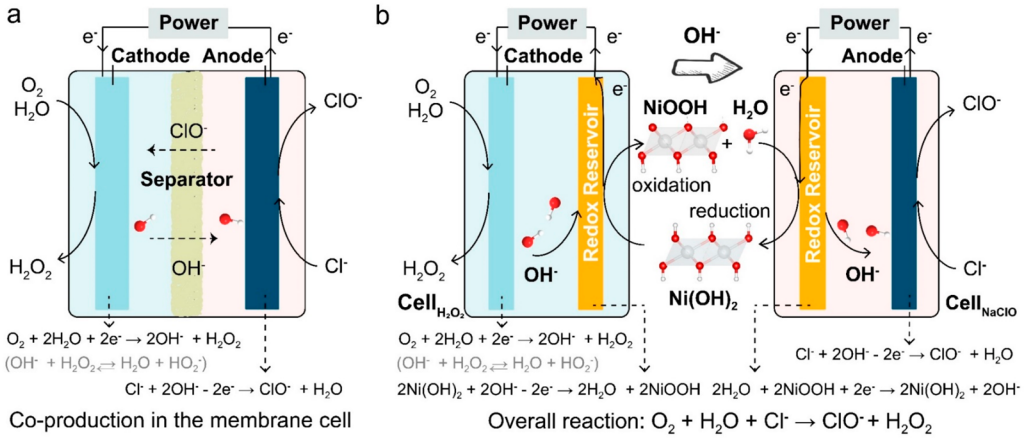

Figure 1. Schematic illustration of ion-balanced ModES production of H_2O_2 and NaClO enabled by an ion-selective RR in comparison with the membrane electrolysis process. (a) In the membrane electrolysis, HPR occurs on the cathode and generates hydroxide ions, along with the hydroxide-consuming HCR on the anode. An anion exchange membrane (AEM) that separates the cathodic and anodic chambers transports OH^- to minimize the pH swing, but ClO^- could also diffuse across the AEM and reacts with H_2O_2 produced at the cathode, which will reduce the overall efficiency. (b) In an ion-balanced ModES system, cathodic and anodic processes are decoupled to produce H_2O_2 and NaClO in different cells. The $Ni(OH)_2$ RR could effectively transport OH^- via the reversible redox conversion with NiOOH to pair up sequentially with the HPR and HCR reactions in two separate cells, denoted as the $Cell_{H_2O_2}$ (left) and $Cell_{NaClO}$ (right). This ion-balanced ModES system can allow sustained coproduction of H_2O_2 and NaClO with stable pH in a batchwise fashion.

cathodic half-reactions. Recent reports have demonstrated decoupling water electrolysis using homogeneous[15−20] or heterogeneous redox mediators[21−26] to improve product separation. ModES using a heterogeneous RR could have a broader impact on on-site electrosynthesis beyond water splitting[14] by pairing half-reactions that are incompatible in conventional membrane electrolysis.[27] Recently, we have demonstrated the coproduction of H_2O_2, sodium persulfate ($Na_2S_2O_8$), and active chlorine (Cl_2, NaClO) in a proof-of-concept ModES system using a nickel hexacyanoferrate (NiHCF) RR.[14] The NiHCF RR could transport Na^+ ions to maintain the charge balance in such coproduction processes; however, the half-reactions either involve OH^- (H_2O_2 and ClO^- production) or solely electron transfer (persulfate production, $2SO_4^{2-} \rightarrow S_2O_8^{2-} + 2e^-$). Even though the RR-enabled ModES strategy could couple two useful half-reactions and avoid product crossover, the mismatch between the ion generation/consumption of the paired half-reactions and the ion transport by the RR results in the imbalance of desired ions and inevitable pH swing.[28] Because of such poor control over ion balance, the previous ModES system could only produce chemicals (H_2O_2, NaClO, and $Na_2S_2O_8$) with limited concentrations, preventing sustained productions and practical applications.

An ideal sustainable electrochemical production process can avoid the sacrificial half-reactions and allow the transport of the desired ions between the two half-reaction processes to maintain the balance of ion carriers. With such an issue in mind, we need to develop an ion-balanced ModES using a better designed RR for sustainable production of disinfectants. Importantly, the cathodic and anodic half-reactions should generate or consume the same ions to maintain the ion balance. The other key is developing and using RR materials that can selectively transport the desired ions to balance the ion generation and consumption involved in the paired half-reactions in ModES. This way, ion balance could be maintained to allow the sustained ModES production of the chemicals enabled by the RR. Here we specifically develop an ion-balanced ModES process using a hydroxide-ion selective $Ni(OH)_2$ RR to produce two widely used disinfectants, H_2O_2 and NaClO, without undesired byproducts and appreciable pH swing. The OH^--consuming oxidation of $Ni(OH)_2$ to NiOOH is coupled with the cathodic H_2O_2 production reaction (HPR) that releases OH^-, while the reduction of NiOOH to $Ni(OH)_2$ generates the OH^- ions for the anodic hypochlorite production reaction (HCR). Redox cycle of the $Ni(OH)_2$ RR effectively transports the OH^- ions from the cathodic cell to the anodic cell to balance the ion generation and consumption associated with the paired half-reactions. We carefully match the OH^--releasing HPR, the OH^--consuming HCR, and the $Ni(OH)_2$ RR to realize an ion-stable electrochemical operation and demonstrate a sustained coproduction of H_2O_2 and NaClO with practically useful concentrations and a high voltage efficiency.

RESULTS AND DISCUSSION

Ion-Balanced ModES System Design and Operations.

To overcome the limitation of the current ModES production due to the imbalanced ion generation and consumption, we design an ion-balanced ModES process to realize the stable coproduction of two widely used disinfectants H_2O_2 and NaClO. A previous study has demonstrated simultaneous HPR [$O_2 + 2H_2O + 2e^- \rightarrow H_2O_2 + 2OH^-$, $E^\circ = 0.267$ V at pH = 7 vs standard hydrogen electrode (SHE)][29] and HCR ($Cl^- \rightarrow Cl_2 + 2e^-$, $E^\circ = 1.36$ V vs SHE, followed by $Cl_2 + 2OH^- \rightarrow H_2O + Cl^- + ClO^-$)[30] in a membrane device,[31] but the crossover of ClO^- ions leads to its reaction with H_2O_2 and results in low Faradaic efficiency (Figure 1a).[31] As illustrated in Figure 1b, the ion-balanced ModES system decouples the simultaneous electrosynthesis into two electrochemical cells and pairs the two individual half-reactions with a RR electrode. The RR electrode, balancing the desired ions associated with the paired half-reactions, requires careful material selection and evaluation. The ideal RR electrodes must meet several criteria: hydroxide-balancing ability, proper redox potential, chemical and electrochemical stability in alkaline and neutral solutions,

https://doi.org/10.1021/acscentsci.1c01157
ACS Cent. Sci. 2021, 7, 2083−2091

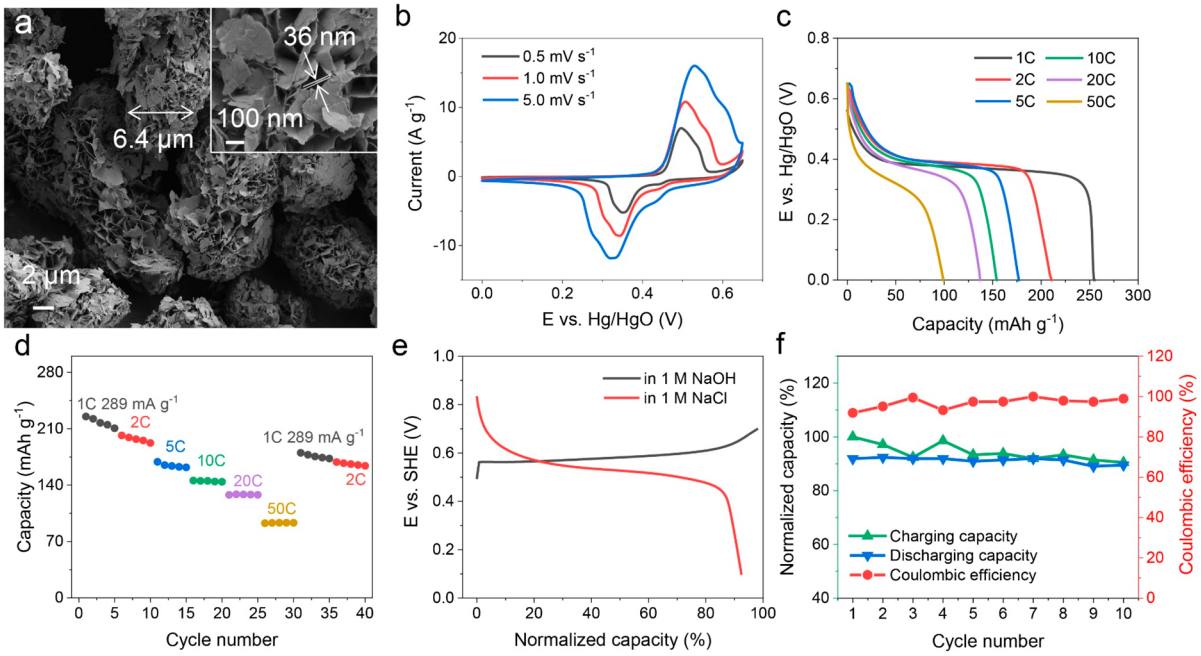

Figure 2. Structural and electrochemical characterizations of the $Ni(OH)_2$RR material. (a) SEM images of the as-synthesized $Ni(OH)_2$ materials. (b) Cyclic voltammograms of the $Ni(OH)_2$ electrode in 1 M NaOH solution at different scan rates from 0.5 to 5 mV s^{-1}. (c) Representative galvanostatic discharge curves of the $Ni(OH)_2$ electrode in 1 M NaOH solution. (d) Rate performance of the $Ni(OH)_2$ electrode (capacity based on active materials). (e) Galvanostatic charge curve of the $Ni(OH)_2$ electrode in 1 M NaOH solution and its galvanostatic discharge curve in 1 M NaCl solution at 10 C rate (2.89 A g^{-1}). Capacity is normalized based on the charging capacity in 1 M NaOH solution. (f) Galvanostatic charge−discharge tests of the $Ni(OH)_2$ electrode with charging in 1 M NaOH solution and discharging in 1 M NaCl solution at 10 C rate (2.89 A g^{-1}).

high capacity, and fast redox kinetics. All the above considerations point to $Ni(OH)_2$/NiOOH electrodes, which have been widely used in alkaline batteries since the end of the 19th century due to their high capacity and good stability.[32] In addition, H_2O_2 solution shows high chemical stability even when mixed with $Ni(OH)_2$ powder (Figure S1). The redox chemistry of $Ni(OH)_2$/NiOOH electrodes follows this equation: $Ni(OH)_2 + OH^- \rightarrow NiOOH + H_2O + e^-$, E° = 0.49 V vs SHE.[33−35]

During a typical ion-balanced ModES cycle, HPR generates OH^- in the cathodic $Cell_{H_2O_2}$, while the RR oxidation from $Ni(OH)_2$ to NiOOH consumes OH^- simultaneously; in the anodic $Cell_{NaClO}$, the RR reduction from NiOOH to $Ni(OH)_2$ generates OH^- as the feedstock for the HCR process (Figure 1b). Like an ion-exchange membrane, $Ni(OH)_2$ RR could maintain the charge balance by consuming or generating OH^- during the redox cycle, thus effectively transporting the OH^- ions from the cathodic cell to the anodic cell. Compared with the paired membrane electrolysis, such a ModES system using an ion-selective RR not only is membrane-free but also avoids the side reactions arising from the product crossover across the membrane. Furthermore, the ion-balanced ModES using an ion-selective RR electrode could minimize the pH shift in electrochemical cells and enable a sustained coproduction of H_2O_2 and NaClO in a batchwise fashion.

Synthesis and Electrochemical Performance of $Ni(OH)_2$ as a Solid-State Redox Reservoir. We synthesized nanostructured $Ni(OH)_2$ via a hydrothermal method without further aging or annealing (see details in Materials and Methods in the Supporting Information).[36] Scanning electron microscopy (SEM) images show the uniform flower-like morphology of $Ni(OH)_2$ with diameters of about 6.4 μm, where each $Ni(OH)_2$ flower is composed of nanoflakes with a thickness around 36 nm (Figure 2a). Powder X-ray diffraction (PXRD) pattern of the as-synthesized $Ni(OH)_2$ (Figure S2a) displays the characteristic (003), (101), and (015) diffraction peaks that match well with the standard pattern of α-$Ni(OH)_2$ (JCPDS no. 38-0715).

We then systematically studied the electrochemical behavior of the as-synthesized α-$Ni(OH)_2$ in 1 M NaOH solution using a three-electrode configuration with a Pt wire counter electrode and a Hg/HgO reference electrode (RE). Before each electrochemical test, we run 20 cycles of galvanostatic charge−discharge (GCD) tests at a 1 C rate to activate the $Ni(OH)_2$ electrodes (Figures S3 and S4). The 1 C rate is defined as 289 mA g^{-1} based on the theoretical capacity (289 mAh g^{-1}) of $Ni(OH)_2$. Note that the α-$Ni(OH)_2$ converts to β-$Ni(OH)_2$ after 20-cycle activation (Figure S2b), and the redox conversion from β-$Ni(OH)_2$ to β-NiOOH can show good reversibility.[37] Cyclic voltammograms (CV) of the $Ni(OH)_2$ electrode at different scan rates from 0.5 to 5 mV s^{-1} (Figure 2b) reveal the excellent reversible redox chemistry arising from Ni^{II}/Ni^{III} redox couple with a formal potential around 0.425 V vs Hg/HgO. The galvanostatic discharging curves of the $Ni(OH)_2$ electrode at different current densities yield the flat discharge plateaus at ∼0.38 V vs Hg/HgO and promise a stable energy output during the reduction process (Figure 2c). Evaluation of the rate capability of the $Ni(OH)_2$ electrode shows that $Ni(OH)_2$ has a high capacity of 225 mAh g^{-1} at 1 C rate with a Coulombic efficiency (CE) above 94%, and the capacity is still 80 mAh g^{-1} at even 50 C with ∼99% CE (Figures 2d and S5). Considering that the oxygen evolution reaction (OER) could occur during the $Ni(OH)_2$ oxidation,[26] the less ideal CE could be attributed to OER during the $Ni(OH)_2$ oxidation process. Galvanostatic cycling tests of the $Ni(OH)_2$ electrode confirm the long-term cycling

https://doi.org/10.1021/acscentsci.1c01157
ACS Cent. Sci. 2021, 7, 2083−2091

stability at different C rates (Figure S6). Significantly, 0.064% decay per cycle was observed at a 10 C rate with an initial capacity of 140 mAh g^{-1}, showing decent durability at a high C rate. Furthermore, the oxidation and reduction of the RR electrode in different electrolytes was evaluated. $Ni(OH)_2$ electrode could be oxidized in alkaline solution but in neither neutral solution nor weak alkaline solution (pH 9−10) (Figure S7 and Figure S8). However, it could be reduced in neutral solution (Figure 2e,f and Table S1). GCD tests with charging in alkaline solution and discharging in neutral solution also show good cycling stability (Figure 2f), suggesting that $Ni(OH)_2$ is suitable as the RR for the ModES production across the neutral and alkaline solutions.

Ion-Balancing Ability of the $Ni(OH)_2$ RR. To evaluate the hydroxide-balancing ability of the $Ni(OH)_2$ RR, we performed three-electrode electrochemical measurements and monitored the pH values of the electrolytes in two distinct cell configurations: the undivided beaker-type cell vs the divided H-cell (left vs right in Figure 3a). The beaker-type cell contains a commercial dimensionally stable anode (DSA) as the WE, a saturated calomel electrode (SCE) as the RE, and a $Ni(OH)_2$ RR electrode as the counter electrode. A glass frit divides the H-cell into two chambers: the left chamber with a $Ni(OH)_2$ RR electrode as the counter electrode, and the right chamber with a DSA electrode as the WE and a SCE as the RE. Notably, the microporous glass frit could slow down the ion movement and primarily allow the major ions (e.g., Na^+ and Cl^- in NaCl solution) to transport between two chambers and maintain the charge balance, which could result in temporary pH shifts in both chambers if the half-reactions on WE and counter electrode involve OH^-. In contrast to the H-cell, all ions, including the minor ions (e.g., OH^- in NaCl solution), could diffuse freely in the beaker-type cell.

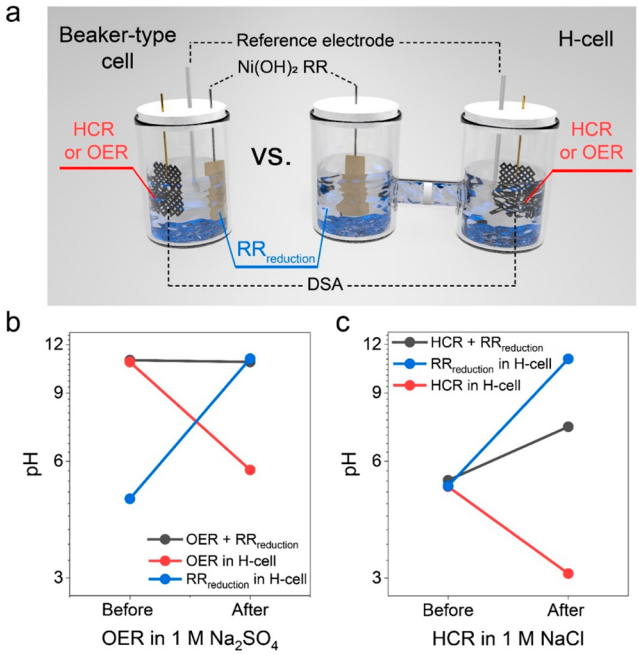

Figure 3. Ion-balancing ability of the $Ni(OH)_2$RR. (a) Illustration of two electrochemical configurations in the beaker-type cell (left) and the H-cell (right) to evaluate the OH^--balancing ability of the $Ni(OH)_2$ RR. All RR electrodes were charged in 1 M NaOH solution before testing the ion-balance ability. (b) pH shift after the OER process in 1 M Na_2SO_4 solution, including the RR reduction (blue) and OER (red) in the H-cell, as well as after the undivided electrolysis in a beaker-type cell (black). (c) pH shift after the HCR process in 1 M NaCl solution, including the RR reduction (blue) and OER (red) in the H-cell, as well as after the undivided electrolysis in a beaker-type cell (black).

We chose two OH^--consuming half-reactions on the DSA electrode, the OER in 1 M Na_2SO_4 solution and HCR in 1 M NaCl solution, as the model half-reactions to study the OH^--balancing ability of the $Ni(OH)_2$ RR. Before running the electrochemical tests of OER (or HCR) paired with RR reduction in 1 M Na_2SO_4 (or 1 M NaCl) solution, the $Ni(OH)_2$ electrode was first oxidized to NiOOH in 1 M NaOH solution (Table S2). Figure 3b,c compares the pH shifts after the OER or HCR processes paired with RR reduction in two cell configurations. Both separated OER and HCR processes lead to a pH decrease (Figure 3b,c, red), suggesting OH^- consumption during these half-reactions. The RR reduction leads to a pH increase (Figure 3b,c, blue), consistent with the following electrode reaction, NiOOH + $H_2O + e^- \rightarrow Ni(OH)_2 + OH^-$. Importantly, we only found a minor pH change from 10.94 to 10.82 in the beak-type cell (Figure 3b, black), where the OH^--generating RR reduction is paired with the OH^--consuming OER. Note that the slight pH swing from 5.36 to 7.36 during the HCR process in the beaker-type cell (Figure 3c, black) could be attributed to the hydrolysis of the formed ClO^- and possibly Cl_2 leak. Because HClO is a weak acid with partial dissociation, and the hydrolysis of the generated ClO^- could generate a little OH^-. The comparison between the small pH shift in the undivided electrolysis and the significant pH decrease in the separated OER and HCR processes demonstrates that the $Ni(OH)_2$ RR could balance the OH^- generation and consumption for the proposed ModES process.

Optimization of Operating Conditions for HPR and HCR. We investigated the H_2O_2 and NaClO production in 1 M NaOH solution (pH = 13.44) and 1 M NaCl solution (at various pH modified by NaOH and HCl), respectively, because of the high activity of the alkaline H_2O_2 production[4] and the effect of pH on the OER activity[38] and the dissociation of ClO^- (Figure S9).[6] For the HCR process, we chose a DSA electrode widely used in the chlor-alkali industry[12,39,40] with reasonable chlorine selectivity[41] as the catalytic electrode. We first tested the HCR in an undivided cell paired with HER to minimize the pH swing and Cl_2 leak due to local pH decrease (Figure S10). CV curve of the DSA electrode shows the current density increased rapidly with the increasing applied voltage or pH (Figure 4a). When the pH is up to 13.3, the onset potential drops to ~0.75 V vs SHE, suggesting that OER becomes the primary reaction rather than HCR (Figure 4a and Figure S11). Figure 4b summarizes the Faradaic efficiency at various pH and applied potentials obtained by chronoamperometry (CA) and followed titration methods (Figure S11, Materials and Methods in the Supporting Information). At the same applied potential, the FE increases from pH = 6.0 to 8.5 and decreases when pH is above 8.5. Specifically, the increased applied potential contributes to a higher FE, with 95.7% at 1.44 V vs SHE and 96.3% at 1.49 V vs SHE in 1 M NaCl solution with a pH of 8.5. These results confirm that the DSA electrode can enable effective HCR process in near-neutral pH.

Among various catalysts for two-electron oxygen reduction reaction (2e⁻ ORR), carbon-based nanomaterials are well-known for low cost and electrochemical stability in neutral and alkaline solutions.[42,43] To boost the HPR activity of the

https://doi.org/10.1021/acscentsci.1c01157
ACS Cent. Sci. 2021, 7, 2083−2091

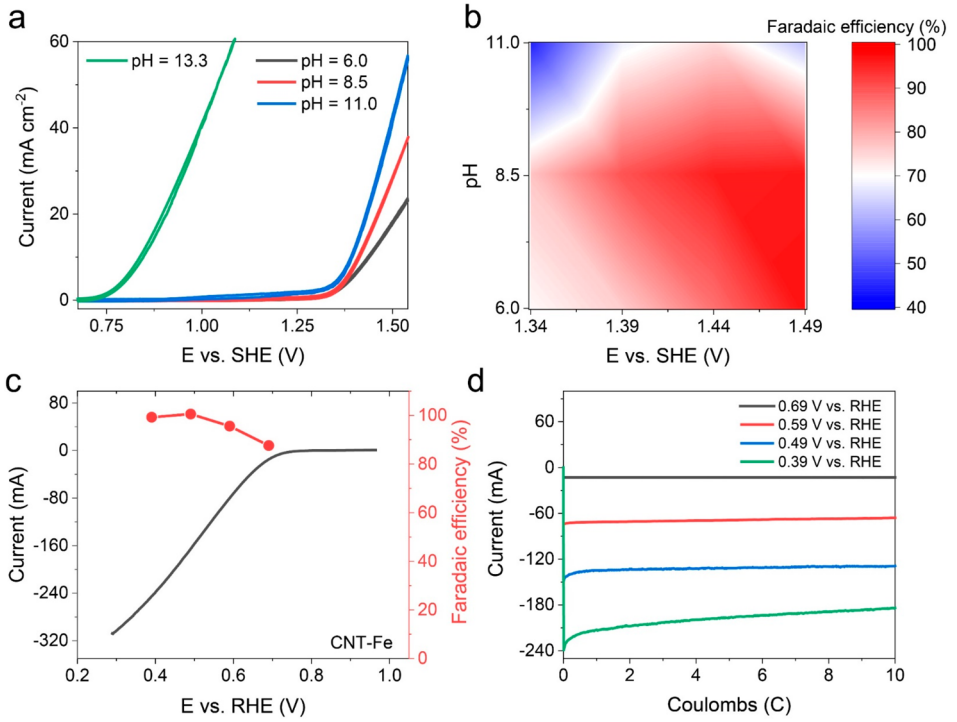

Figure 4. Investigation of the separated electrochemical H_2O_2 and NaClO production in conventional cells. (a) Cyclic voltammograms of the DSA electrode at a scan rate of 10 mV s^{-1} in 1 M NaCl solution with different pH. (b) Faradaic efficiency of HCR by DSA electrode at various pH and applied potentials in 1 M NaCl solution (interpolated from 12 data points). (c) Linear scanning voltammetry (LSV) curve of the Fe-CNT electrode with an electrode area of 1 cm^2 at 10 mV s^{-1} in O_2-saturated 1 M NaOH solution and the corresponding potential-dependent Faradaic efficiency for HPR. (d) Chronoamperometry (CA) curves of the Fe-CNT electrode for the H_2O_2 production at various applied potentials in O_2-saturated 1 M NaOH solution.

pristine carbon nanotube (CNT), we modified commercial multiwalled carbon nanotubes (MWCNTs, ~10 nm width, Figure S12) via an Fe-atom decoration method (Fe-decorated CNT noted as Fe-CNT),[44] because it was reported that the Fe−C−O motif is more favorable to the $2e^-$ ORR than $4e^-$ ORR. No atomic clusters were observed in the transmission electron microscopy (TEM) images (Figure S12), and no obvious transition metal signals were detected in these CNT samples by X-ray photoelectron spectroscopy (XPS, Figure S13), suggesting low Fe-mass loading and well-dispersed metal atoms.[44] The Fe-CNT electrode was prepared on the Teflon-treated carbon fiber paper (1 cm^2 area) with a mass loading around 0.2 mg by a drop-casting method and then evaluated in a divided H-cell filled with 1 M NaOH solution (Figure S10). The linear scanning voltammetry (LSV) curve of the Fe-CNT electrode shows a high current of −308 mA at 0.39 V vs RHE (Figure 4c), corresponding to a mass activity, 1544 A g^{-1} at 0.39 V vs RHE. This is 2 times higher than that of the pristine CNT electrode (−109 mA, Figure S14), revealing the improved ORR activity after the atomic decoration. The FE of HPR is determined by chronoamperometry and a chemical titration method (Figure S15, Materials and Methods in the Supporting Information). Both Fe-CNT and CNT electrodes show high FE above 90% in the potential range from 0.39 to 0.69 V vs RHE (Figure 4c and Figure S16). Moreover, stable bulk electrolysis is demonstrated by the CA curves of the Fe-CNT electrode for the cumulative HPR (Figure 4d), confirming the excellent activity and stability of the Fe-CNT catalysts.

Ion-Balanced ModES Production of H_2O_2 and NaClO. We then demonstrated an ion-balanced ModES system using a $Ni(OH)_2$ RR in two electrochemical cells for the sustainable production of H_2O_2 and NaClO. Both ModES processes were performed in the undivided beaker-type cell with a three-electrode configuration (see details in Materials and Methods and Figures S17−18). The typical two-step ModES cycle is investigated by the chronopotentiometry method with an applied current of 60 mA. As shown in Figure 5a, in the $Cell_{H_2O_2}$, HPR on the Fe-CNT electrode exhibits an average potential of ~ −0.27 V vs SHE, and the RR electrode is oxidized from RR^{red} to RR^{ox} until 0.8 V vs SHE. After washing with NaCl solution, the RR^{ox} is reduced back to RR^{red} to finish one ModES cycle in the $Cell_{NaClO}$, while HCR on the DSA electrode shows an average potential of ~1.48 V vs SHE. The Faradaic efficiencies of HPR and HCR are calculated based on the produced H_2O_2 and NaClO in each cell (Materials and Methods). During the coproduction, the average potential difference between the catalytic electrodes and the RR electrode determines the average cell voltages (E_{cell}). To describe the energy utilization of the ion-balanced ModES, we use the voltage efficiency (VE) defined for the aqueous electrosynthesis system[14] based on the following equation:

$$\begin{aligned} \mathrm{VE}(\%) &= E_{\mathrm{DIR}}/E_{\mathrm{ModES}} \times 100\% \\ &= (E_{\mathrm{NaClO}} + E_{\mathrm{H_2O_2}} - \Delta V)/(E_{\mathrm{NaClO}} + E_{\mathrm{H_2O_2}}) \\ &\quad \times 100\% \end{aligned}$$

where E_{DIR} is the potential difference between the HPR on the Fe-CNT electrode and HCR on the DSA electrode, respectively ($E_{DIR} = E_{NaClO} + E_{H_2O_2} - \Delta V = 1.71$ V); ΔV is the potential difference between the average potential of RR

https://doi.org/10.1021/acscentsci.1c01157
ACS Cent. Sci. 2021, 7, 2083−2091

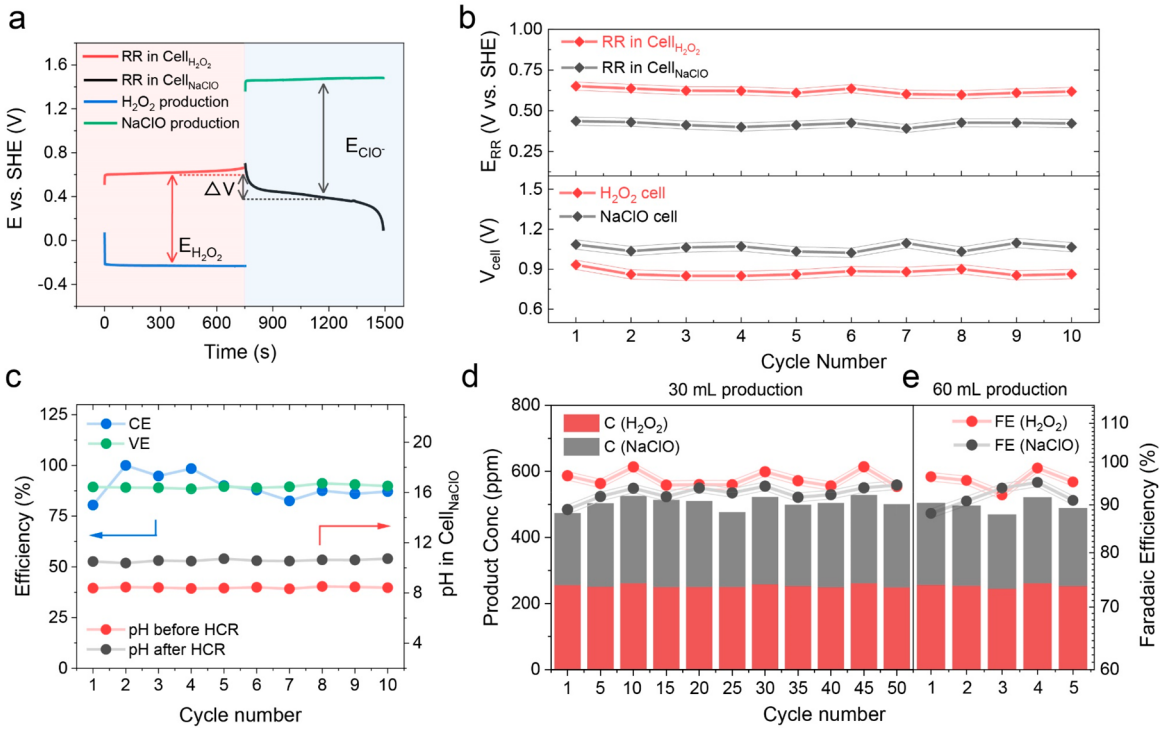

Figure 5. Sustained modular electrosynthesis of H_2O_2 and NaClO in an ion-balanced ModES system enabled by a $Ni(OH)_2$RR. (a) Chronopotentiometry curves of the electrodes in the $Cell_{H_2O_2}$ and $Cell_{NaClO}$ at 60 mA. The RR oxidation (red) was paired with HPR (blue) in 1 M NaOH solution, and the RR reduction (black) was paired with HCR (green) in 1 M NaCl solution with pH = 8.5. The ΔV represents the average potential difference between the RR oxidation and RR reduction. (b) Average potential of the RR electrode (E_{RR}, top) and the corresponding average cell voltages (E_{cell}, bottom) of the $Cell_{H_2O_2}$ and $Cell_{NaClO}$ in 10-cycle ion-balanced ModES processes in 30 mL solution. (c) CE of RR, VE, and pH shift in the $Cell_{NaClO}$ over ten ModES cycles in 30 mL solution. Modular coproduction of H_2O_2 and NaClO at (d) 30 mL (for 50 cycles using a 61 mg RR electrode) and (e) 60 mL scale (for 5 cycles using a 136.9 mg RR electrode), showing the product concentration up to 251 ppm (red column) and 481 ppm (gray column), as well as the Faradaic efficiencies (red and black scatters) for each ModES cycle (selected cycles for the 50-cycle process).

oxidation and that of the RR reduction. Specifically, the E_{ModES} is 1.93 V for this coproduction, and total VE is up to 88.6% even under a large applied current.

Considering the natural H_2O_2 decomposition due to unstable peroxide chemistry,[45,46] we optimized the HPR production with the RR oxidation under various theoretical product concentrations. After changing the charge input (Q_{input}) for HPR using the RR electrodes with different mass loading, we found the theoretical concentration increased linearly with increasing Q_{input} (Figure S19). The same trend occurs when the actual H_2O_2 concentration is from 0 to 250 ppm with a FE above 95%. However, the FE drops to 50% when the theoretical concentration is 550 ppm, reflecting the inevitable H_2O_2 decomposition in a highly concentrated H_2O_2 solution. To further understand the H_2O_2 oxidation reaction, CV and LSV of the $Ni(OH)_2$ electrodes are carried out in 1 M NaOH solutions containing various concentrations of H_2O_2. The increased anodic area from CV curve in 1 M NaOH solution with 300 ppm of H_2O_2 than that in 1 M NaOH solution indicates the H_2O_2 decomposition, and the smaller cathodic area also suggests the electrocatalytic oxidation (Figure S20a). As the H_2O_2 concentration increases, the *iR*-corrected LSV profiles exhibit an increasing trend at a fixed applied potential, indicating a faster decomposition rate at higher H_2O_2 concentration (Figure S20b). The relatively low CE from GCD tests also confirms the undesired H_2O_2 oxidation. As a result, keeping the H_2O_2 concentration below 300 ppm could effectively minimize the electrochemical decomposition of H_2O_2.

We then investigated the continuous ModES production of H_2O_2 and NaClO at 60 mA by cycling the same RR electrode (60 mg, 45 Coulombs per cycle). During the 10-cycle production in 30 mL solution, the average RR potential (E_{RR}) in the $Cell_{H_2O_2}$ stays at 0.66 V vs SHE with a fluctuation of ±0.03 V (Figure 5b, top, red, and Figure S21), which is likely due to oxygen bubbling in 1 M NaOH solution. The E_{RR} in the $Cell_{NaClO}$ remains at 0.42 V vs SHE with a variation of ±0.04 V (Figure 5b, top, black, and Figure S21), which is perhaps influenced by the local pH swing during HCR. The corresponding E_{cell} shows average values of 0.97 and 1.02 V in the $Cell_{H_2O_2}$ and $Cell_{NaClO}$ (Figure 5b, bottom). Over the 10-cycle production, the ion-balanced ModES system delivers an average CE of RR about 89.5% and VE of 89.5% (Figure 5c), in agreement with the representative ModES cycle above (Figure 5a). Significantly, we found a repeatable pH increase from ∼8.44 to ∼10.57 during each HCR cycle rather than a pH decrease (Figure 5c), confirming the OH^--balance ability of the $Ni(OH)_2$ RR. The pH increase also indicates that HCR did not entirely consume the OH^- generated by the RR electrode, which could be possibly due to the Cl_2 leak resulting from the low local pH around the DSA electrode. The larger-scale ModES production in 60 mL solution (using a larger RR electrode with a mass loading of 136.9 mg and 90 Coulombs per cycle) also showed a high CE, VE, and repeatable pH

https://doi.org/10.1021/acscentsci.1c01157
ACS Cent. Sci. 2021, 7, 2083−2091

increase (Figures S22 and S23), consistent with the small-scale production.

Furthermore, Figure 5d shows the 50-cycle continuous ModES production of the two disinfectants in a 30 mL solution (using a 61 mg RR electrode, 45 Coulombs per cycle) (complete details in Figures S24 and S25). Figure 5e shows the ModES processes in a 60 mL solution for 5 cycles without appreciable degradation in the FE and product concentration (complete details in Figures S22 and S23). The $Ni(OH)_2$ RR also shows a high utilization of capacity up to 96.6% over the ModES processes (Figure S24 and Table S3). Note that after 50 cycle ModES processes, the $Ni(OH)_2$ RR has the β-$Ni(OH)_2$ structure and shows no obvious structural change, which further confirms the good stability of the $Ni(OH)_2$ RR (Figure S2b). The small fluctuations of FE and product concentration between these cycles perhaps result from the variation of the charge passing through each electrochemical cell and the potential changes of the catalytic reactions arising from the oxygen bubbling and small local pH swing. Consequently, this ion-balanced ModES system could produce practically useful H_2O_2 and NaClO with concentrations up to 251 and 481 ppm, respectively, confirming the sustained electrochemical synthesis without sacrificial auxiliary reactions.

Design Principles of Effective Ion-Balanced ModES. The ion-balanced ModES coproduction of H_2O_2 and NaClO is successfully demonstrated based on the following design principles. First, just like the conventional anode−cathode coupled electrolysis, suitable half-reactions are the basis for establishing a successful ion-balanced ModES process, especially considering that different half-reactions often require various reaction conditions (e.g., solvent and the solution pH). To achieve sustained electrosynthesis, we must carefully consider the ion generation and consumption involved in the two half-reactions. Electrochemical half-reactions, such as cathodic/anodic reactions and RR half-reactions, are either proton/hydroxide-coupled or non-proton/hydroxide-coupled. The HPR and HCR processes here both involve OH^-: $O_2 + 2H_2O + 2e^- \rightarrow H_2O_2 + 2OH^-$,[47] and $Cl^- + 2OH^- - 2e^- \rightarrow ClO^- + H_2O$.[6] When these ion-matched reactions are paired in ModES, the HPR process generates OH^- to balance the OH^--consuming HCR, contributing to a byproduct-free paired electrosynthesis: $O_2 + H_2O + Cl^- \rightarrow H_2O_2 + ClO^-$.

More importantly, the key to ion-balanced ModES process is developing and employing ion-selective RRs to decouple the desired half-reactions and selectively transport the target ion carriers between these half-reactions. The ion selectivity of RR materials always depends on their redox mechanism. For example, porous carbon with the capacitive behavior[48] shows weak ion selectivity, while Bi and Ag with a conversion mechanism exhibit high selectivity on halide ions.[49] The $Ni(OH)_2$ RR electrode demonstrated here shows OH^--consuming oxidation from $Ni(OH)_2$ to NiOOH, while the reduction of NiOOH to $Ni(OH)_2$ generates OH^-. Based on the redox conversion between $Ni(OH)_2$ and NiOOH,[35] the $Ni(OH)_2$ RR could effectively transport the OH^- ions and enable the OH^--balanced coproduction of H_2O_2 and NaClO. Therefore, RR materials that could selectively transport the desired ions to balance the ion generation and consumption are crucial to successful ion-balanced ModES processes.

To ensure an efficient ModES process, it is necessary to study the stability of targeted electrosynthesis product chemicals because they are often electrochemically sensitive and could be reduced or oxidized in practical electrolysis.[50] Here we examined the concentration threshold of the H_2O_2 produced from HPR to reduce possible oxidation of it, achieving a high FE in the ModES processes. Moreover, the average potential difference (ΔV, or the voltage hysteresis) between the RR oxidization and reduction should be small to maximize the VE. Here we used around 100% state-of-charge (SOC) of the RR electrode with a 0.22 V ΔV and achieved an 88.6% VE during the ion-balanced ModES processes. Generally speaking, the RR material with an excellent rate capability will have a small ΔV,[51] suggesting a promising way to improve VE by enhancing RR's redox kinetics. Another important principle for an effective ModES process is to match the current passing through the electrocatalysts and the RR materials. The battery electrode-like RR materials display decreasing capacity and larger voltage hysteresis as the current increases, resulting in a smaller VE. On the other hand, varying current by changing the applied potential can also influence the FE of the electrosynthesis half-reactions (Figure 4c). Therefore, low current does not necessarily guarantee a high overall energy efficiency for the ModES process because the half-reactions could suffer from a low FE under such conditions. Thus, effective ion-balanced ModES processes could be designed based on a proper current matching between the half-reactions and the RRs. The ion-balanced ModES demonstrated here is limited to aqueous electrosynthesis, especially the OH^--related chemistry.[30,47] With the exploration of more energy storage materials as ion-selective RRs and additional electrosynthesis reactions, ion-balanced ModES processes can be suitable for distributed electrochemical manufacturing of a broader range of chemicals. Given that physically moving the RR electrodes among different cells is not very practical for industrial applications, developing a continuous-flow ModES system beyond the laboratory demonstration based on batch processing will be desirable.[14,22,24,26]

CONCLUSION

In conclusion, we demonstrated an ion-balanced ModES strategy by integrating the electrochemical productions of two widely used disinfectants, H_2O_2 and NaClO, using $Ni(OH)_2$ as the ion-selective RR. Because the $Ni(OH)_2$ RR could selectively balance the OH^- generation and consumption associated with the paired HPR and HCR processes, we achieved sustained coproduction of these chemicals with stable operation and nonappreciable pH swing, which allowed the accumulation of H_2O_2 and NaClO up to practically useful concentrations of 251 and 481 ppm, respectively. In contrast to the conventional electrosynthesis of disinfectants, the ion-balanced ModES system pairing two otherwise incompatible half-reactions could produce two valuable chemicals without sacrificial auxiliary reactions and unwanted byproducts. In addition, following the design principles illustrated here, the voltage efficiency of the ModES could be further boosted by choosing RRs with faster redox kinetics or optimizing the current matching between the electrosynthesis half-reactions and the RRs. To facilitate and further improve such ion-balanced ModES processes, it is crucial to develop and evaluate new heterogeneous RRs tailored for the targeted ModES production of chemicals. Furthermore, the ion-balanced ModES strategy using an ion-selective RR could facilitate process intensification by making use of both the oxidative and reductive equivalents in an electrochemical process without lengthy process optimizations. Such a modular approach could

https://doi.org/10.1021/acscentsci.1c01157
ACS Cent. Sci. 2021, 7, 2083−2091

facilitate on-demand distributed electrochemical manufacturing of a diversity of chemicals at different scales.

■ ASSOCIATED CONTENT

Supporting Information

The Supporting Information is available free of charge at https://pubs.acs.org/doi/10.1021/acscentsci.1c01157.

Materials and methods, materials characterizations, and additional figures and tables on electrochemical measurements (PDF)

■ AUTHOR INFORMATION

Corresponding Author

Song Jin − *Department of Chemistry, University of Wisconsin-Madison, Madison, Wisconsin 53706, United States;* orcid.org/0000-0001-8693-7010; Email: jin@chem.wisc.edu

Authors

Rui Wang − *Department of Chemistry, University of Wisconsin-Madison, Madison, Wisconsin 53706, United States;* orcid.org/0000-0001-5554-6519

Hongyuan Sheng − *Department of Chemistry, University of Wisconsin-Madison, Madison, Wisconsin 53706, United States;* orcid.org/0000-0002-0494-4418

Fengmei Wang − *Department of Chemistry, University of Wisconsin-Madison, Madison, Wisconsin 53706, United States; CAS Key Laboratory of Nanosystem and Hierarchical Fabrication, National Center for Nanoscience and Technology, Beijing 100190, P. R. China;* orcid.org/0000-0002-9438-9859

Wenjie Li − *Department of Chemistry, University of Wisconsin-Madison, Madison, Wisconsin 53706, United States;* orcid.org/0000-0001-9216-0922

David S. Roberts − *Department of Chemistry, University of Wisconsin-Madison, Madison, Wisconsin 53706, United States;* orcid.org/0000-0002-0478-4987

Complete contact information is available at: https://pubs.acs.org/10.1021/acscentsci.1c01157

Notes

The authors declare no competing financial interest.

■ ACKNOWLEDGMENTS

This work is supported by a University of Wisconsin-Madison UW2020 Grant by the Wisconsin Alumni Research Foundation (WARF). F. W. also thanks the fellowship support by China Scholarship Council (CSC, 201804910251). The authors gratefully acknowledge use of facilities and instrumentation supported by NSF through the University of Wisconsin Materials Research Science and Engineering Center (DMR-1720415). We also thank Prof. Shannon Stahl and Dr. James Gerken for helpful discussion.

■ REFERENCES

(1) US EPA: Disinfectants for Use Against SARS-CoV-2. https://www.epa.gov/pesticide-registration/list-n-disinfectants-use-against-sars-cov-2 (accessed Dec 2, 2021).

(2) US CDC: Disinfection and Sterilization. https://www.cdc.gov/infectioncontrol/guidelines/disinfection/index.html (accessed Dec 2, 2021).

(3) Black and Veatch Corporation. Chlorine: History, Manufacture, Properties, Hazards, and Uses. In *White's Handbook of Chlorination and Alternative Disinfectants*, 5th ed.; Dominic, M.; Desiderio, N. M., Eds.; John Wiley & Sons, Inc: New Jersey, 2009; pp 1−67.

(4) Campos-Martin, J. M.; Blanco-Brieva, G.; Fierro, J. L. G. Hydrogen peroxide synthesis: an outlook beyond the anthraquinone process. *Angew. Chem., Int. Ed.* **2006**, *45*, 6962−6984.

(5) Moussallem, I.; Jörissen, J.; Kunz, U.; Pinnow, S.; Turek, T. Chlor-alkali electrolysis with oxygen depolarized cathodes: history, present status and future prospects. *J. Appl. Electrochem.* **2008**, *38*, 1177−1194.

(6) Black and Veatch Corporation. Hypochlorination—Sodium Hypochlorite. In *White's Handbook of Chlorination and Alternative Disinfectants*, 5th ed., Dominic, M.; Desiderio, N. M., Eds.; John Wiley & Sons, Inc: New Jersey, 2009; pp 452−527.

(7) Baldea, M.; Edgar, T. F.; Stanley, B. L.; Kiss, A. A. Modular manufacturing processes: Status, challenges, and opportunities. *AIChE J.* **2017**, *63*, 4262−4272.

(8) Langlois, R. N. Modularity in technology and organization. *J. Econ Behav Organ* **2002**, *49*, 19−37.

(9) Seifert, T.; Sievers, S.; Bramsiepe, C.; Schembecker, G. Small scale, modular and continuous: A new approach in plant design. *Chem. Eng. Process.* **2012**, *52*, 140−150.

(10) Shao, Y.; Zavala, V. M. Modularity measures: Concepts, computation, and applications to manufacturing systems. *AIChE J.* **2020**, *66*, No. e16965.

(11) Zichittella, G.; Pérez-Ramírez, J. Status and prospects of the decentralised valorisation of natural gas into energy and energy carriers. *Chem. Soc. Rev.* **2021**, *50*, 2984−3012.

(12) Matousek, R. Hypochlorite Synthesis Cells and Technology, Sea Water. In *Encyclopedia of Applied Electrochemistry*, 2014 ed., Kreysa, G.; Ota, K.-i.; Savinell, R. F., Eds.; Springer New York: New York, 2014; pp 1066−1070.

(13) SANILEC. https://denora.com/products/brands/SANILEC.html (accessed Dec 2, 2021).

(14) Wang, F.; Li, W.; Wang, R.; Guo, T.; Sheng, H.; Fu, H.-C.; Stahl, S. S.; Jin, S. Modular Electrochemical Synthesis Using a Redox Reservoir Paired with Independent Half-Reactions. *Joule* **2021**, *5*, 149−165.

(15) Symes, M. D.; Cronin, L. Decoupling hydrogen and oxygen evolution during electrolytic water splitting using an electron-coupled-proton buffer. *Nat. Chem.* **2013**, *5*, 403−9.

(16) Rausch, B.; Symes, M. D.; Chisholm, G.; Cronin, L. Decoupled catalytic hydrogen evolution from a molecular metal oxide redox mediator in water splitting. *Science* **2014**, *345*, 1326−1330.

(17) Li, W.; Jiang, N.; Hu, B.; Liu, X.; Song, F.; Han, G.; Jordan, T. J.; Hanson, T. B.; Liu, T. L.; Sun, Y. Electrolyzer Design for Flexible Decoupled Water Splitting and Organic Upgrading with Electron Reservoirs. *Chem.* **2018**, *4*, 637−649.

(18) Huang, J.; Xie, Y.; Yan, L.; Wang, B.; Kong, T.; Dong, X.; Wang, Y.; Xia, Y. Decoupled amphoteric water electrolysis and its integration with Mn−Zn battery for flexible utilization of renewables. *Energy Environ. Sci.* **2021**, *14*, 883−889.

(19) Wang, F.; Sheng, H.; Li, W.; Gerken, J. B.; Jin, S.; Stahl, S. S. Stable Tetrasubstituted Quinone Redox Reservoir for Enhancing Decoupled Hydrogen and Oxygen Evolution. *ACS Energy Lett.* **2021**, *6*, 1533−1539.

(20) Chen, J.-J.; Symes, M. D.; Cronin, L. Highly reduced and protonated aqueous solutions of $[P_2W_{18}O_{62}]^{6-}$ for on-demand hydrogen generation and energy storage. *Nat. Chem.* **2018**, *10*, 1042−1047.

(21) Chen, L.; Dong, X.; Wang, Y.; Xia, Y. Separating hydrogen and oxygen evolution in alkaline water electrolysis using nickel hydroxide. *Nat. Commun.* **2016**, *7*, 11741.

(22) Landman, A.; Dotan, H.; Shter, G. E.; Wullenkord, M.; Houaijia, A.; Maljusch, A.; Grader, G. S.; Rothschild, A. Photoelectrochemical water splitting in separate oxygen and hydrogen cells. *Nat. Mater.* **2017**, *16*, 646−651.

(23) Ma, Y.; Dong, X.; Wang, Y.; Xia, Y. Decoupling Hydrogen and Oxygen Production in Acidic Water Electrolysis Using a Poly-

triphenylamine-Based Battery Electrode. *Angew. Chem., Int. Ed.* **2018**, *57*, 2904−2908.
(24) Dotan, H.; Landman, A.; Sheehan, S. W.; Malviya, K. D.; Shter, G. E.; Grave, D. A.; Arzi, Z.; Yehudai, N.; Halabi, M.; Gal, N.; Hadari, N.; Cohen, C.; Rothschild, A.; Grader, G. S. Decoupled hydrogen and oxygen evolution by a two-step electrochemical−chemical cycle for efficient overall water splitting. *Nat. Energy* **2019**, *4*, 786−795.
(25) Ma, Y.; Guo, Z.; Dong, X.; Wang, Y.; Xia, Y. Organic Proton-Buffer Electrode to Separate Hydrogen and Oxygen Evolution in Acid Water Electrolysis. *Angew. Chem., Int. Ed.* **2019**, *58*, 4622−4626.
(26) Landman, A.; Halabi, R.; Dias, P.; Dotan, H.; Mehlmann, A.; Shter, G. E.; Halabi, M.; Naseraldeen, O.; Mendes, A.; Grader, G. S. Decoupled photoelectrochemical water splitting system for centralized hydrogen production. *Joule* **2020**, *4*, 448−471.
(27) Paidar, M.; Fateev, V.; Bouzek, K. Membrane electrolysis—History, current status and perspective. *Electrochim. Acta* **2016**, *209*, 737−756.
(28) Zeng, J. S.; Manthiram, K. Redox Reservoirs: Enabling More Modular Electrochemical Synthesis. *Trends Chem.* **2021**, *3*, 157.
(29) Yang, S.; Verdaguer-Casadevall, A.; Arnarson, L.; Silvioli, L.; Čolić, V.; Frydendal, R.; Rossmeisl, J.; Chorkendorff, I.; Stephens, I. E. Toward the decentralized electrochemical production of H2O2: a focus on the catalysis. *ACS Catal.* **2018**, *8*, 4064−4081.
(30) Hou, M.; Chen, L.; Guo, Z.; Dong, X.; Wang, Y.; Xia, Y. A clean and membrane-free chlor-alkali process with decoupled Cl_2 and H_2/NaOH production. *Nat. Commun.* **2018**, *9*, 438.
(31) Kalu, E. E.; Oloman, C. Simultaneous electrosynthesis of alkaline hydrogen peroxide and sodium chlorate. *J. Appl. Electrochem.* **1990**, *20*, 932−940.
(32) McBreen, J. Nickel Hydroxides. In *Handbook of Battery Materials*, 2nd ed., Daniel, C.; Brendenbach, J. O., Eds.; Wiley-VCH Verlag GmbH & Co. KGaA: Weinheim, 2011; pp 149−168.
(33) Bode, H.; Dehmelt, K.; Witte, J. Zur kenntnis der nickelhydroxidelektrode—I. Über das nickel (II)-hydroxidhydrat. *Electrochim. Acta* **1966**, *11*, 1079−1087.
(34) Bode, H.; Dehmelt, K.; Witte, J. Zur kenntnis der nickelhydroxidelektrode. II. Über die oxydationsprodukte von nickel (ii) hydroxiden. *Z. Anorg. Allg. Chem.* **1969**, *366*, 1−21.
(35) Shukla, A. K.; Hariprakash, B., Secondary Batteries − Nickel Systems | Electrodes: Nickel. In *Encyclopedia of Electrochemical Power Sources*, Garche, J., Ed.; Elsevier: Amsterdam, 2009; pp 404−411.
(36) Jiang, H.; Zhao, T.; Li, C.; Ma, J. Hierarchical self-assembly of ultrathin nickel hydroxide nanoflakes for high-performance supercapacitors. *J. Mater. Chem.* **2011**, *21*, 3818.
(37) Hall, D. S.; Lockwood, D. J.; Bock, C.; MacDougall, B. R. Nickel hydroxides and related materials: a review of their structures, synthesis and properties. *Proc. R. Soc. London, Ser. A* **2015**, *471*, 20140792.
(38) Yang, Y.; Dang, L.; Shearer, M. J.; Sheng, H.; Li, W.; Chen, J.; Xiao, P.; Zhang, Y.; Hamers, R. J.; Jin, S. Highly active trimetallic NiFeCr layered double hydroxide electrocatalysts for oxygen evolution reaction. *Adv. Energy Mater.* **2018**, *8*, 1703189.
(39) Trieu, V.; Schley, B.; Natter, H.; Kintrup, J.; Bulan, A.; Hempelmann, R. RuO_2-based anodes with tailored surface morphology for improved chlorine electro-activity. *Electrochim. Acta* **2012**, *78*, 188−194.
(40) Duby, P. The history of progress in dimensionally stable anodes. *JOM* **1993**, *45*, 41−43.
(41) Karlsson, R. K. B.; Cornell, A. Selectivity between Oxygen and Chlorine Evolution in the Chlor-Alkali and Chlorate Processes. *Chem. Rev.* **2016**, *116*, 2982−3028.
(42) Zhang, X.; Xia, Y.; Xia, C.; Wang, H. Insights into Practical-Scale Electrochemical H_2O_2 Synthesis. *Trends Chem.* **2020**, *2*, 942−953.
(43) Lu, Z.; Chen, G.; Siahrostami, S.; Chen, Z.; Liu, K.; Xie, J.; Liao, L.; Wu, T.; Lin, D.; Liu, Y.; Jaramillo, T. F.; Nørskov, J. K.; Cui, Y. High-efficiency oxygen reduction to hydrogen peroxide catalysed by oxidized carbon materials. *Nat. Catal* **2018**, *1*, 156−162.
(44) Jiang, K.; Back, S.; Akey, A. J.; Xia, C.; Hu, Y.; Liang, W.; Schaak, D.; Stavitski, E.; Norskov, J. K.; Siahrostami, S.; Wang, H. Highly selective oxygen reduction to hydrogen peroxide on transition metal single atom coordination. *Nat. Commun.* **2019**, *10*, 3997.
(45) Lin, S.-S.; Gurol, M. D. Catalytic decomposition of hydrogen peroxide on iron oxide: kinetics, mechanism, and implications. *Environ. Sci. Technol.* **1998**, *32*, 1417−1423.
(46) Haber, F.; Weiss, J. The catalytic decomposition of hydrogen peroxide by iron salts. *Proc. Math. Phys. Eng. Sci.* **1934**, *147*, 332−351.
(47) Sheng, H.; Hermes, E. D.; Yang, X.; Ying, D.; Janes, A. N.; Li, W.; Schmidt, J. R.; Jin, S. Electrocatalytic Production of H_2O_2 by Selective Oxygen Reduction Using Earth-Abundant Cobalt Pyrite (CoS_2). *ACS Catal.* **2019**, *9*, 8433.
(48) Zhang, L. L.; Zhao, X. Carbon-based materials as supercapacitor electrodes. *Chem. Soc. Rev.* **2009**, *38*, 2520−2531.
(49) Chen, F.; Leong, Z. Y.; Yang, H. Y. An aqueous rechargeable chloride ion battery. *Energy Storage Mater.* **2017**, *7*, 189−194.
(50) Francke, R.; Little, R. D. Redox catalysis in organic electrosynthesis: basic principles and recent developments. *Chem. Soc. Rev.* **2014**, *43*, 2492−2521.
(51) Dreyer, W.; Jamnik, J.; Guhlke, C.; Huth, R.; Moškon, J.; Gaberšček, M. The thermodynamic origin of hysteresis in insertion batteries. *Nat. Mater.* **2010**, *9*, 448−453.

https://doi.org/10.1021/acscentsci.1c01157
ACS Cent. Sci. 2021, 7, 2083−2091